Analysis of the Vibration Characteristics of a Permanent Magnet Motor with an Inclined Rotor

Ao Zhang, He Li*

Northeastern University, Shenyang, China

Abstract: For most permanent magnet motors, the noise of motors are mainly excites by the unbalanced magnetic pull (UMP) of rotors, and the eccentricity is the most common trouble sources in the rotor system. This paper studied the effect of an inclined rotor on the vibration characteristics in a magnet motor. Three dimensional analytical model of the internal magnetic field of the motor was built based on the theory of electromagnetic field, and the analytical model of UMP was obtained and substituted into motion equation of rotor system. The numerical simulation was conducted by Matlab, and the dynamic response of the system under the action of UMP and unbalanced mass eccentricity was obtained. Through several illustrating numerical examples, the effects of different parameters on the vibration of an eccentric rotor system were discussed in detail. The results showed that different parameters have important effects on the rotor system, and this provided a theoretical basis for the structural design of the rotor of permanent magnet motor and the maintenance of the motor.

Keywords: UMP; Inclined rotor; Vibration characteristics

1 Introduction

With the advantages of simple structure, good performance and high efficiency, the permanent magnet motor has been widely used in various fields. In the motor operation process, the rotor eccentricity exists due to unbalanced mass eccentricity, wear of bearings and shaft bending. The rotation of the eccentric rotor changes the air-gap field and produces an unbalanced magnetic pull (UMP) [1]. The UMP can affect the working environment of bearings and cause some more severe vibrations [2]. When the UMP increases to a certain value, the magnetic force pulls the rotor to the stator, which causes rubbing between the rotor and stator, and then damages the motor [3].

Many researchers have studied the UMP with the analytical method and the finite element method in the past decades [4-8]. The linear equations were often used in the engineering field, and this method can cause large error when the eccentricity is large. Werner [9] developed a rotor dynamic model in an induction motor with an eccentric rotor, and derived a calculation method for evaluating the vibration sensitivity. Some researchers have introduced nonlinear methods to study the UMP. Guo [10] adopted the simplified Fourier series method to calculate the UMP and analyzed the effects on the

*Corresponding Author: He Li (hli@mail.neu.edu.cn)

vibration in a three-phase generator with eccentric rotor. Li [11] studied the radial magnetic forces in permanent magnet motors having rotor eccentricity, and introduced a new analytical model for studying the relationship between eccentricity effect and design parameters of slotted permanent magnet motors. Im [12] analyzed the dynamic behaviors of a BLDC motor when the motor undergoes mechanical and electromagnetic interaction by considering the air gap variation, and derived new equations. Michon et al. [13] studied the effects of rotor eccentricity on the UMP and induced electromotive forces in permanent magnet, and the results shown the UMP can be of similar or greater magnitude than the gravitational force acting on the rotor. The rotor eccentricity can be divided into three categories—static eccentricity, dynamic eccentricity and incline eccentricity—which is caused by rotor uneven misalignment in axial direction. Most of the researches were focused on the static eccentricity or dynamic eccentricity, and they analyzed the problems in a plane. However, as Fig.1 shows, the incline eccentricity always exists due to some extent, and this means the detailed analysis should be concentrated on the incline eccentricity.

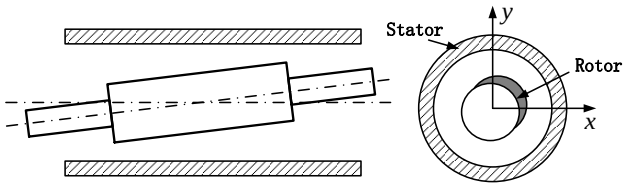

Fig. 1. An inclined rotor.

Recently, some researchers have studied the incline UMP in the motors. Dorrell [14, 15] analyzed the UMP in large induction machines with incline eccentricity, and used the stator damper windings to reduce the UMP. Yu [16] presented an analytical model for analyzing effects of the UMP induced by the misalignment rotor in PMSM. Di [17] proposed a new method to calculate the UMP in cage induction motors, considering the curved dynamic eccentricity, and used the finite element method for verification. Although the analysis of the UMP in an inclined rotor has been studied in these researches, the effects on the vibration characteristics have been rarely analyzed. This paper presents a three dimensional analytical model of the UMP, considering the inclined eccentricity of the rotor. The dynamic response of the rotor system under the action of UMP and unbalanced mass eccentricity are analyzed by the numerical method, and the static parameters are analyzed for their effects on the dynamic responses. Then some conclusions are proposed.

2 Dynamic model of the rotor system

2.1 Analysis of the air-gap length

When describing the rotor state, we use a set of parameters: the static parameters $(x_0, y_0, \theta_{x0}, \theta_{y0})$ and the dynamic parameters $(x, y, \theta_x, \theta_y)$. The parameters (x_0, y_0) and $(\theta_{x0}, \theta_{y0})$ are the static displacement eccentricity and angle eccentricity, (x, y) and

ISSN 2572-4975 (Print), 2572-4991 (Online)

(θ_x, θ_y) are the dynamic displacement eccentricity and angle eccentricity. In order to describe the geometric relationships between the rotor and the stator, the geometric figure can be simplified as shown in Fig. 2. The coordinate system $O-XYZ$ is for the stator and the coordinate system $o-xyz$ is for the rotor.

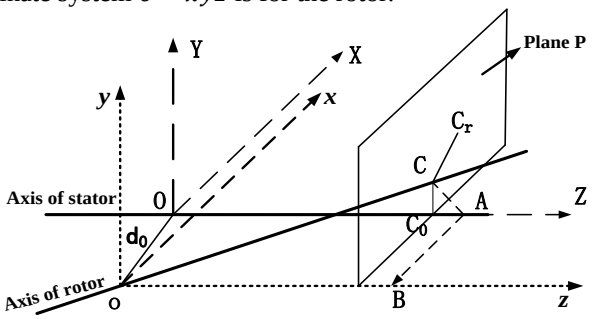

Fig. 2. Geometric relationships between the rotor and the stator.

According to Fig. 2, point A is selected on the coordinate axis OZ and B is the point corresponding to A on the coordinate axis oz. The following expressions can be expressed as:

$$\boldsymbol{OA} = \ （0,0,\mathrm{Z}） \tag{1}$$

$$\boldsymbol{oB} = \ （0,0,\mathrm{Z}） \tag{2}$$

In order to analyze the position of the rotor, the Euler angle is used to describe the space motion. The transformation matrices of rotation around the axis ox and oy can be written as follows, when considering both the static angle eccentricity θ_{x0}, θ_{y0} and the dynamic angle eccentricityθ_x, θ_y.

$$\boldsymbol{R}_{ox} = \begin{pmatrix} \cos(\theta_{y0}+\theta_y) & 0 & \sin(\theta_{y0}+\theta_y) \\ 0 & 1 & 0 \\ -\sin(\theta_{y0}+\theta_y) & 0 & \cos(\theta_{y0}+\theta_y) \end{pmatrix} \tag{3}$$

$$\boldsymbol{R}_{oy} = \begin{pmatrix} 1 & 0 & 0 \\ 0 & \cos(\theta_{x0}+\theta_x) & -\sin(\theta_{x0}+\theta_x) \\ 0 & \sin(\theta_{x0}+\theta_x) & \cos(\theta_{x0}+\theta_x) \end{pmatrix} \tag{4}$$

After the coordinate rotation, the coordinate of point C can be obtained from point B.

$$\begin{pmatrix} x_{oC} \\ y_{oC} \\ z_{oC} \end{pmatrix} = \boldsymbol{R} \cdot \begin{pmatrix} 0 \\ 0 \\ \mathrm{Z} \end{pmatrix} = \boldsymbol{R}_{oy}\boldsymbol{R}_{ox} \begin{pmatrix} 0 \\ 0 \\ \mathrm{Z} \end{pmatrix} \tag{5}$$

Then the vector $\boldsymbol{oC}$ can be described as follows:

$$\boldsymbol{oC} = (Z\cos(\theta_{x0}+\theta_x)\sin(\theta_{y0}+\theta_y), -Z\sin(\theta_{x0}+\theta_x), Z\cos(\theta_{x0}+\theta_x)\cos(\theta_{y0}+\theta_y)) \tag{6}$$

Since vector $\boldsymbol{Oo}$ in Fig. 2 can be written as:

$$\boldsymbol{Oo} = (x_0, y_0, 0) \tag{7}$$

Then the vector $\boldsymbol{OC}$ can be described as follows:

$$\boldsymbol{OC} = (x_0 + Z\cos(\theta_x+\theta_{x0})\sin(\theta_y+\theta_{y0}), y_0 - Z\sin(\theta_x+\theta_{x0}), Z\cos(\theta_{x0}+\theta_x)\cos(\theta_{y0}+\theta_y)) \tag{8}$$

In order to calculate the air-gap length along the axis oz, the plane P containing point C is parallel to the OXY plane. Then the coordinates of C_0 can be calculated as follows [18]:

$$\boldsymbol{OC_0} = (0,0,Z\cos(\theta_{x0}+\theta_x)\cos(\theta_{y0}+\theta_y)) \quad (9)$$

$$\boldsymbol{C_0C} = (x_0 + Z\cos(\theta_x+\theta_{x0})\sin(\theta_y+\theta_{y0}), y_0 - Z\sin(\theta_x+\theta_{x0}),0) \quad (10)$$

The plane P is selected for better analysis of the air-gap length between the stator and the rotor. As Fig. 3 shows, C_0 is the center of the stator, C is the center of the rotor under the static state and C_r is the center of the rotor during the operation state. The distance between C and C_r is r, which is determined by the dynamic response and $r = \sqrt{x^2+y^2}$. θ is the position angle of rotor and $\cos\theta = x/r$, $\sin\theta = y/r$. α is the air-gap angle with respect to axis ox.

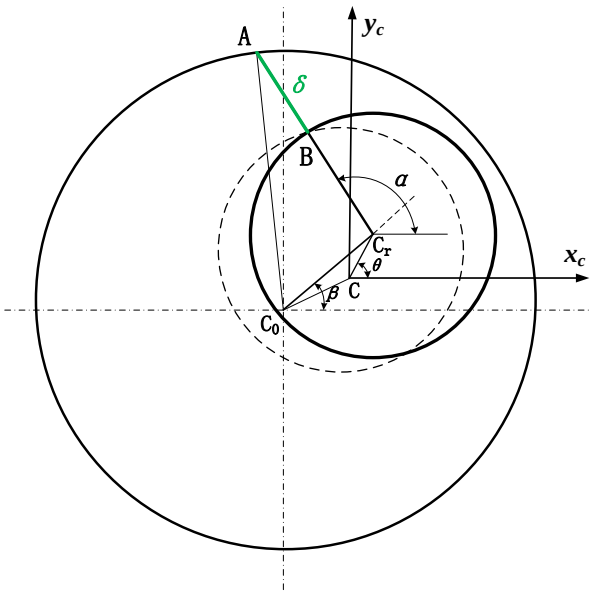

Fig. 3. Air-gap length of the rotor.

According to vector $\boldsymbol{C_0C}$ and $\boldsymbol{CC_r}$, vector $\boldsymbol{C_0C_r}$ can be obtained as:

$$\boldsymbol{C_0C_r} = \boldsymbol{C_0C} + \boldsymbol{CC_r} = (x + x_0 + Z\cos(\theta_x+\theta_{x0})\sin(\theta_y+\theta_{y0}), y + y_0 - Z\sin(\theta_x+\theta_{x0}),0) \quad (11)$$

Then the comprehensive eccentricity e can be written as:

$$e = |\boldsymbol{C_0C_r}| = \sqrt{[x + x_0 + Zcos(\theta_x+\theta_{x0})sin(\theta_y+\theta_{y0})]^2 + [y + y_0 - Zsin(\theta_x+\theta_{x0})]^2} \quad (12)$$

where β is the direction angle of the comprehensive eccentricity and

$$\beta = \begin{cases} \arccos\left[\frac{x+x_0+Z\cos(\theta_{x0}+\theta_x)\sin(\theta_{y0}+\theta_y)}{e}\right] & (y + y_0 - Z\sin(\theta_{x0}+\theta_x) \geq 0) \\ 2\pi - \arccos\left[\frac{x+x_0+Z\cos(\theta_{x0}+\theta_x)\sin(\theta_{y0}+\theta_y)}{e}\right] & (y + y_0 - Z\sin(\theta_{x0}+\theta_x) < 0) \end{cases} \quad (13)$$

ISSN 2572-4975 (Print), 2572-4991 (Online)

As Fig. 3 shows, the air-gap length δ in this moment can be expressed as:

$$\delta(\alpha, t, z) = l_{\mathrm{AB}} = l_{\mathrm{AC}_r} - r \tag{14}$$

Based on cosine theorem, l_{AC_r} can be written as:

$$l_{\mathrm{AC}_r} = \sqrt{R^2 - e^2 \sin^2(\alpha - \beta)} - e \cdot \cos(\alpha - \beta) \tag{15}$$

Considering $e^2 \ll R^2$:

$$l_{\mathrm{AC}_r} \approx R - e \cdot \cos(\alpha - \beta) \tag{16}$$

Then the air-gap length δ can be expressed as:

$$\delta(\alpha, t, z) = R - r - e \cdot \cos(\alpha - \beta) = \delta_0 - e \cdot \cos(\alpha - \beta) \tag{17}$$

where δ_0 is the air-gap length when the rotor is centered.

Taking the effects of permanent magnets into consideration, δ_0 should be written as the effective air-gap length δ':

$$\delta' = \delta_0 + h_m/\mu_r \tag{18}$$

where h_m is the thickness of the magnet and μ_r is the relative recoil permeability.

Then the air-gap length of inclined rotor in the three-dimensional space can be expressed as:

$$\delta'(\alpha, t, z) = \delta' - e \cdot \cos(\alpha - \beta) \tag{19}$$

2.2 The magnetic flux density of the air-gap

The instantaneous air-gap field distribution can be calculated by summing the open-circuit field produced by the permanent magnet and the armature reaction field generated by the winding. The radial air-gap magnetic field of DC motors can be expressed as follows, when the rotor is centered[19-22].

$$B_r(\alpha, t) = [\sum_{n=1,3,5\cdots}^{\infty} B_{mr} \cos np(\alpha - \omega_r t) + \sum_{m=1}^{\infty} B_{ar} \cos(N_0 m\alpha - \omega_e t + \varphi)] \cdot \tilde{\lambda} \tag{20}$$

where p is the number of pole-pair, B_{mr} is the amplitude of the open-circuit field, B_{ar} is the amplitude of the armature reaction field and $\tilde{\lambda}$ is the relative permeance.

Since the permeance is inversely proportional to the air-gap length, the correction factor $\varepsilon_{\delta s}$ can be obtained as follows [23]:

$$\varepsilon_{\delta s}(\alpha, t, z) = \frac{\delta'}{\delta'(\alpha, t, z)} = \frac{1}{1 - \varepsilon' \cos(\alpha - \beta)} \tag{21}$$

where ε' is the effective eccentricity, and $\varepsilon' = e/\delta'$.

The correction factor can be expanded as a Fourier series:

$$\varepsilon_{\delta s}(\alpha, t, z) = \sum_{k=0}^{\infty} \varepsilon_k \cos k(\alpha - \beta) \tag{22}$$

The Fourier coefficients ε_k are

$$\varepsilon_k = \begin{cases} \frac{1}{\sqrt{1-\varepsilon'^2}}, & k = 0; \\ \frac{2}{\sqrt{1-\varepsilon'^2}} \left(\frac{1-\sqrt{1-\varepsilon'^2}}{\varepsilon'}\right)^k, & k = 1,2,3,\ldots; \end{cases} \tag{23}$$

When the eccentricity is small, only the first-harmonic component and the second-harmonic component need to be taken into account. Then the correction factor can be written as

$$\varepsilon_{\delta s}(\alpha,t,z)=\frac{1}{\sqrt{1-\varepsilon'^2}}+\frac{2}{\sqrt{1-\varepsilon'^2}}\left(\frac{1-\sqrt{1-\varepsilon'^2}}{\varepsilon'}\right)\cos(\alpha-\beta) \tag{24}$$

Based on the above analysis, the radial magnetic flux density distribution of the air-gap in the three-dimensional space can be expressed as:

$$B_{rs}(\alpha,t,z)=B_r(\alpha,t)\ \varepsilon_{\delta s}(\alpha,t,z) \tag{25}$$

2.3 The differential equations of the rotor system

The Maxwell stress on the rotor surface can be written as

$$\sigma(\alpha,t,z)=\frac{B_{rs}^2(\alpha,t,z)}{2\mu_0} \tag{26}$$

where μ_0 is the vacuum magnetic permeability.

When the rotor is inclined, the effective air-gap axial length becomes short. According to equation (9), the effective axial length can be expressed as

$$z=Z\cos(\theta_{x0}+\theta_x)\cos\left(\theta_{y0}+\theta_y\right),\quad Z\in[-L/2\,,L/2] \tag{27}$$

where L is the axial length of the rotor.

The UMP of the rotor in the x-direction and y-direction can be calculated by integrating the Maxwell stress:

$$F_{xUMP}=r\int_{\frac{-l}{2}}^{\frac{l}{2}}\int_0^{2\pi}\sigma(\alpha,t,z)\cos\alpha\ d\alpha\ dz \tag{28}$$

$$F_{yUMP}=r\int_{\frac{-l}{2}}^{\frac{l}{2}}\int_0^{2\pi}\sigma(\alpha,t,z)\sin\alpha\ d\alpha\ dz \tag{29}$$

where r is the radius of the rotor and l is the axial length of the air-gap. And l can be written as

$$l=L\cos(\theta_x+\theta_{x0})\cos(\theta_y+\theta_{y0}) \tag{30}$$

The electromagnetic torque can be calculated as follows:

$$M_{xUMP}=-r\int_{\frac{-l}{2}}^{\frac{l}{2}}z\int_0^{2\pi}\sigma(\alpha,t,z)\sin\alpha\ d\alpha\ dz \tag{31}$$

$$M_{yUMP}=r\int_{\frac{-l}{2}}^{\frac{l}{2}}z\int_0^{2\pi}\sigma(\alpha,t,z)\cos\alpha\ d\alpha\ dz \tag{32}$$

The unbalanced mass excitation of the rotor can be obtained as

$$F_x=ma\,\omega^2\cos\omega t \tag{33}$$

$$F_y=ma\omega^2\sin\omega t \tag{34}$$

where m is the mass of the rotor, a is the mass eccentricity, ω is the rotating angular frequency of the rotor and $\omega=2\pi\Omega$ in which Ω is the rotating frequency.

As Fig. 4 shows, the rotor system adopts a Jeffcott rotor for analysis. The rotor is not in the middle of the shaft and the gyroscopic effect need to be considered. L_b is the distance between the left bearing and right bearing, and L_r is the position of rotor.

ISSN 2572-4975 (Print), 2572-4991 (Online)

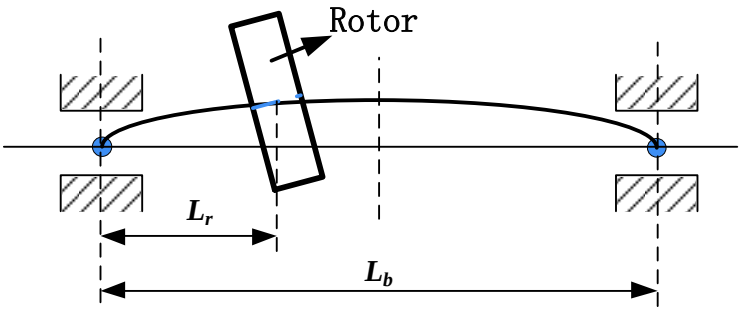

Fig. 4. Schematic of rotor system.

The differential equations of the rotor system in Fig.4 can be expressed as

$$\begin{cases} m\ddot{x} + c_{11}\dot{x} + k_{11}x + k_{14}\theta_y = F_x + F_{xUMP} \\ m\ddot{y} + c_{22}\dot{y} + k_{22}y - k_{23}\theta_x = F_y + F_{yUMP} - mg \\ J_d\ddot{\theta}_x + H\dot{y} - k_{32}y + k_{33}\theta_x = M_{xUMP} \\ J_d\ddot{\theta}_y - H\dot{y} + k_{41}y + k_{44}\theta_y = M_{yUMP} \end{cases}$$

where c_{11} and c_{22} are the damping coefficients. $k_{ij}(i,j = 1,2,3,4)$ are the stiffness coefficients, and $k_{11} = k_{22}$, $k_{14} = k_{23} = k_{32} = k_{41}$, $k_{33} = k_{44}$. J_d is the diametral moment of inertia and $J_d = 1/4\,mR^2$. H is the moment of momentum and $H = J_p\,\omega$, which $J_p = 2J_d$ is the polar moment of inertia.

3 Numerical simulation analysis

Due to the nonlinear characteristics of the system, the numerical simulation is conducted by Matlab, and the differential equations are solved by the explicit fourth-order Runge–Kutta formula with fixed step size. The parameters are as follows: m=15kg, p=2, μ_r=1.05, $\mu_0 = 4\pi\times10^{-7}$, r=0.048m, δ_0=0.006m, h_m=0.006m, L=0.1m, $c_{11} = c_{22} =$ 80Ns/m, $k_{11} = k_{22} = 1.769\times10^6$ N/m, $k_{33} = k_{44} = 1.474\times10^5$ N/m, $k_{14} = k_{23} = k_{32} = k_{41} = -2.949\times10^5$N/m, Ω=10Hz, f=50Hz, $a = 5\times10^{-4}$m.

3.1 Effects of unbalanced mass eccentricity

The mass eccentricity of rotor always exists due to many factors, which means the centroid and barycenter of rotor are not coincide. The rotor shaft orbits for the different mass eccentricities are as Fig. 5 shows. It is seen from Fig. 5(a) that the rotor shaft orbit is not concentric when the mass eccentricity is zero due to the influence of gravity. It is also seen that the displacement responses increase with the mass eccentricity and in order to reduce the dynamic response, the mass eccentricity need to be as small as possible. The shaft orbits from Fig. 5(b), (c) are irregular under the influence of centrifugal force and then become regular in Fig. 5(d) for the centrifugal force plays a dominant role with the increase of mass eccentricity.

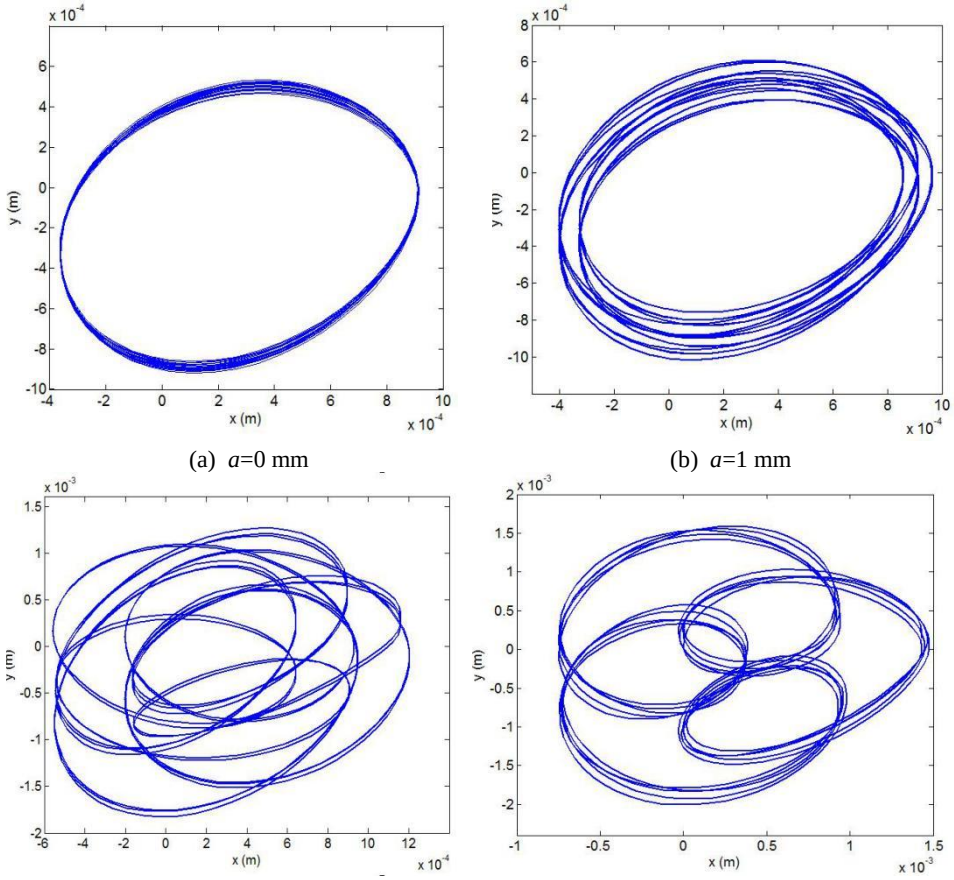

(a) a=0 mm (b) a=1 mm

(c) a=5 mm (d) a=10 mm

Fig. 5. Rotor shaft orbit with different mass eccentricities.

3.2 Effects of static eccentricities

Static eccentricity always exists due to many factors and it can be divided into two categories: displacement eccentricity (x_0, y_0) and angle eccentricity $(\theta_{x0}, \theta_{y0})$. In this paper, x_0 and θ_{x0} is selected to analyze the effects on the vibration characteristics of the rotor system.

The dynamic responses with different displacement eccentricities can be seen in Fig. 6 when the static angle eccentricity is equal to zero. It can be seen that the dynamic responses $(x, y, \theta_x, \theta_y)$ increase with the increase of static displacement eccentricity. According to the analysis of section 2, the UMP and electromagnetic torque depend on the static eccentricity and their values change with the increase of static displacement eccentricity. Thus, the change of static displacement eccentricity can have an effect on the dynamic responses.

 ISSN 2572-4975 (Print), 2572-4991 (Online)

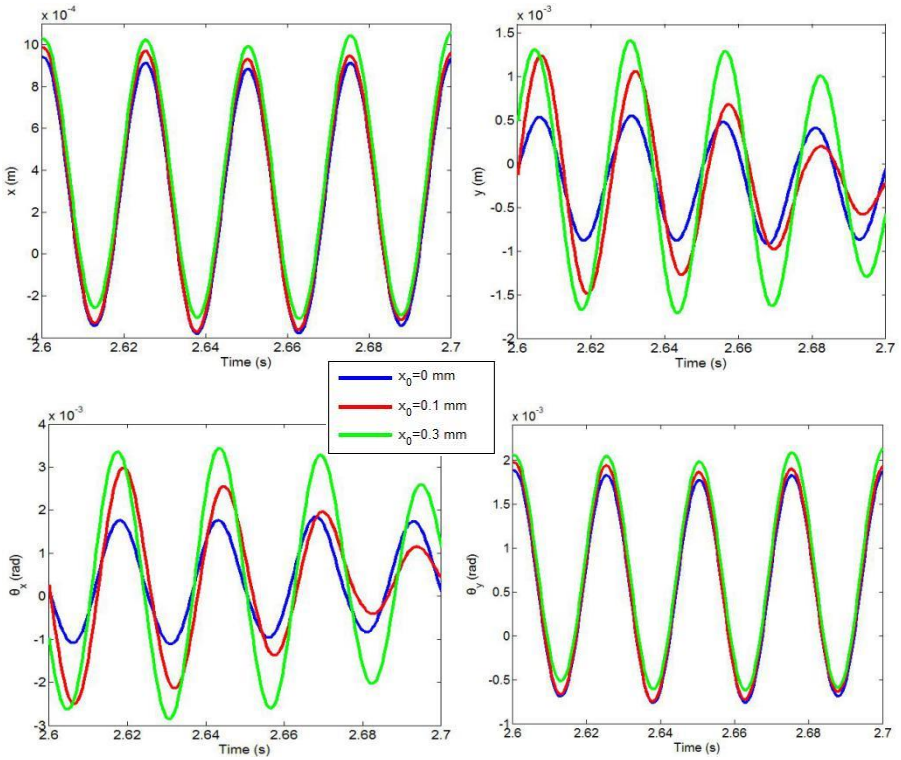

Fig. 6. Time history of the dynamic responses for different static displacement eccentricities.

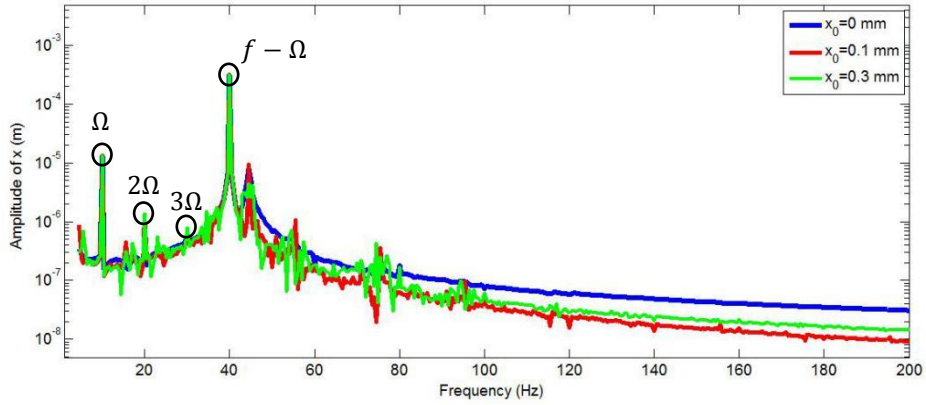

Fig. 7. The spectra of *x* for different static displacement eccentricities.

The spectra of the dynamic displacement response (*x*) for different static displacement eccentricities are shown in Fig. 7. The frequencies in the figure contain the integral multiples of rotating frequency (10Hz) and the combination of rotating frequency and electrical frequency (50Hz). This combined frequency comes from the coupling effects of the rotating rotor and the armature reaction in the stator. It can be seen that the highest integer multiples of rotating frequency increase with the static

displacement eccentricities and more frequency components appear in larger static displacement eccentricity. From the above analysis, large static eccentricity produces large dynamic responses, and this can excite more frequency components. Therefore, to provide a better working condition, the static displacement eccentricity should to be as small as possible.

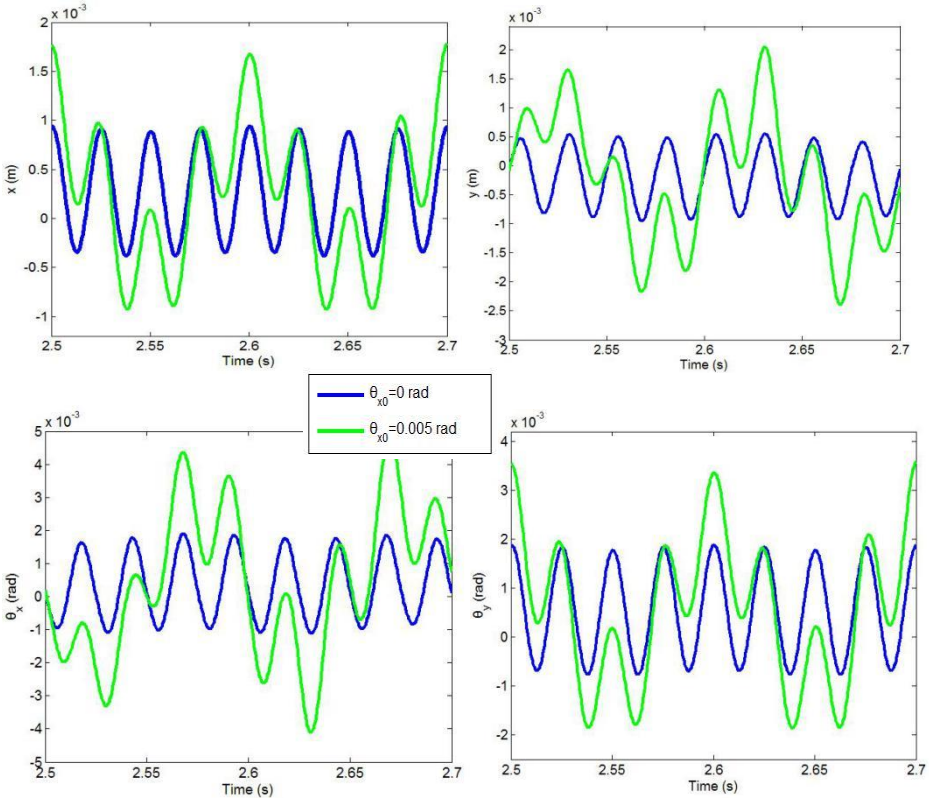

Fig. 8. Time history of the dynamic responses for different static angle eccentricities.

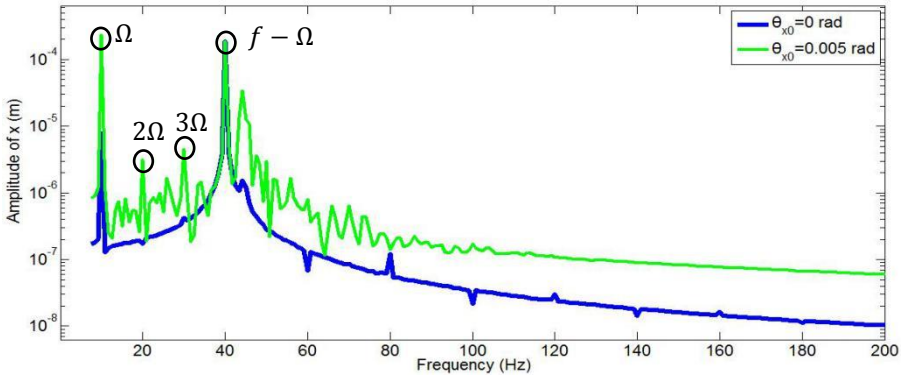

Fig. 9. The spectra of *x* for different static angle eccentricities.

ISSN 2572-4975 (Print), 2572-4991 (Online)

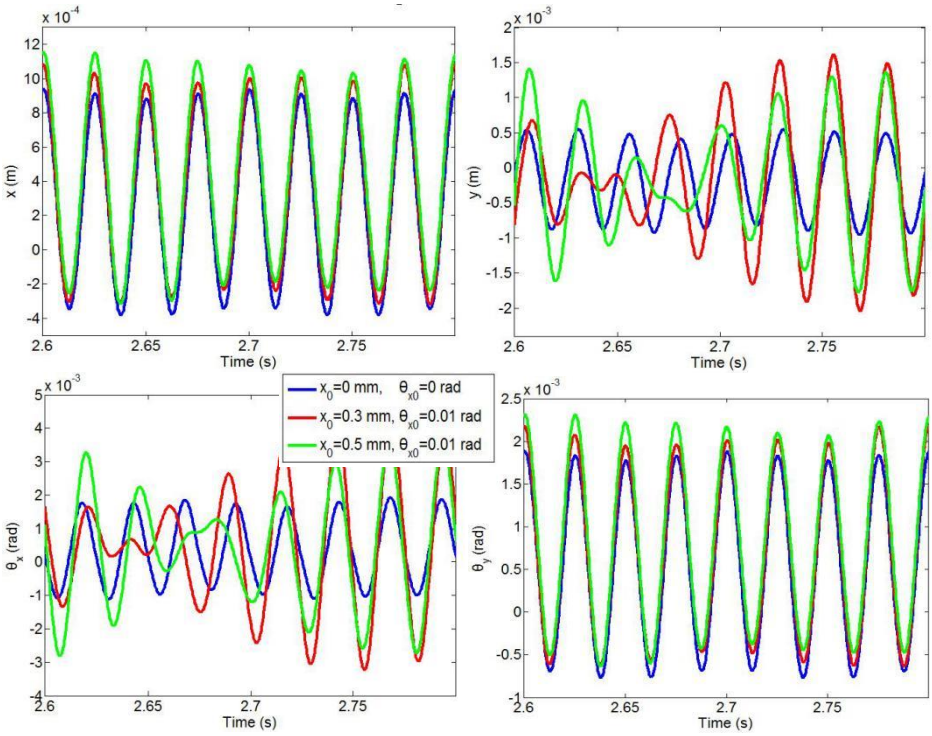

Fig. 10. Time history of the dynamic responses for different static displacement eccentricities when the static angle eccentricity is same.

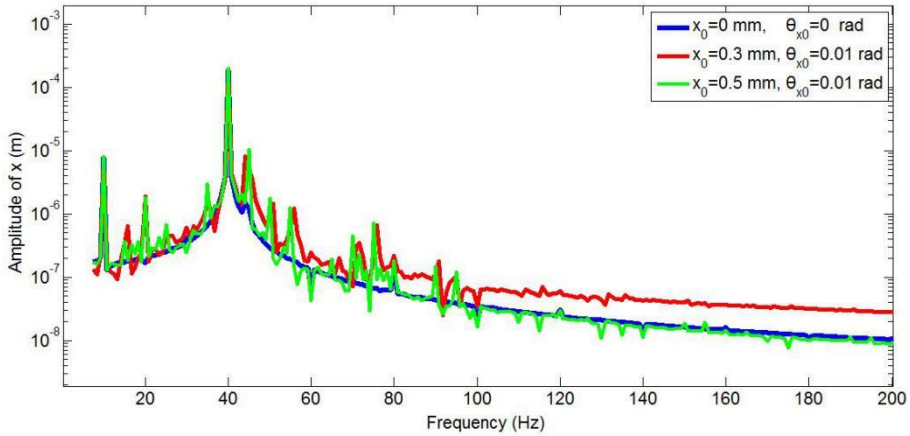

Fig. 11. The spectra of *x* for different static displacement eccentricities when the static angle eccentricity is same.

The dynamic responses with different static angle eccentricities can be seen in Fig. 8 when the static displacement eccentricity is equal to zero. It can be seen that the static angle eccentricity has a significant effect on the dynamic responses $(x, y, \theta_x, \theta_y)$. It shows that large static angle eccentricity can produce large dynamic responses, which

is similar with the static displacement eccentricity. It also can be seen from Fig. 9 that the frequencies contain the integral multiples of rotating frequency and the combination of rotating frequency and electrical frequency, and more frequency components appear due to the existence of static angle eccentricity. In this case, the static angle eccentricity needs to be avoided in the operation of the machine.

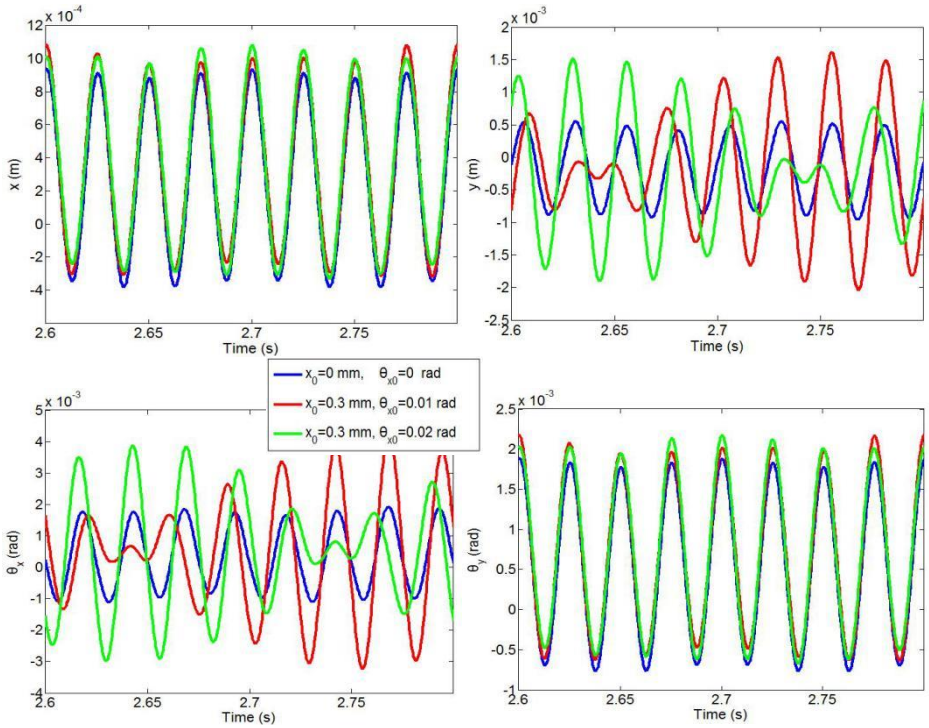

Fig. 12. Time history of the dynamic responses for different static angle eccentricities when the static displacement eccentricity is same.

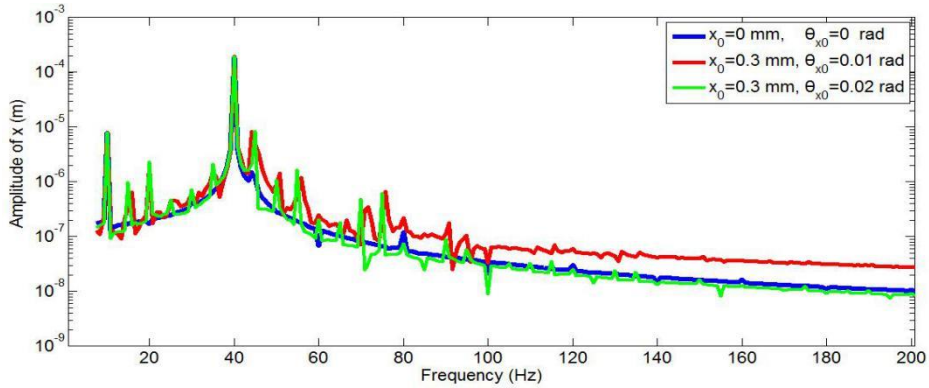

Fig. 13. The spectra of *x* for different static angle eccentricities when the static displacement eccentricity is same.

ISSN 2572-4975 (Print), 2572-4991 (Online)

The rotor with both the static displacement eccentricity and static angle eccentricity is more common in the actual operation. Thus, the effects of this situation need to be analyzed in detail. The dynamic responses with different static displacement eccentricities are shown in Fig. 10 when the static angle eccentricity is same. It can be seen that the dynamic displacement response x and the dynamic angle response θ_y increase with the static displacement eccentricity. It also can be seen that the dynamic displacement response y and the dynamic angle response θ_x change without regularity due to the influence of gravity, and this influence will be studied in the following investigation. The spectral characteristics of the dynamic displacement response (x) in this case are displayed in Fig. 11, and the frequency components also contain the integral multiples of rotating frequency and the combination of rotating frequency and electrical frequency. It also can be seen that more frequency components appear when both the static displacement eccentricity and static angle eccentricity exist.

The dynamic responses and the spectral characteristics of the dynamic displacement response (x) with different static angle eccentricities are shown in Fig. 12 and Fig. 13 when the static displacement eccentricity is same. It can be observed that the dynamic responses are not much different with Fig. 10 and the spectral characteristics in Fig. 13 are roughly at the same. It can be indicated that both the static displacement eccentricity and static angle eccentricity have a great effect on the dynamic responses, and more frequency components can be excited in this situation.

4 Conclusions

A three dimensional analytical model of a permanent magnet motor with an inclined rotor was presented and the dynamic responses of the rotor system under the action of UMP and unbalanced mass eccentricity were analyzed by the numerical method. The static displacement eccentricity and angle eccentricity were analyzed for their effects on the vibration characteristics of the rotor system. The conclusions can be summarized as follows:

(1) The dynamic displacement responses increase with the mass eccentricity. The electromagnetic force plays a dominant role when the mass eccentricity is small and the centrifugal force become more important with the increase of mass eccentricity.
(2) The static displacement eccentricity and the static angle eccentricity can enlarge the amplitudes of dynamic responses, respectively. The frequencies of dynamic responses contain the integral multiples of rotating frequency and the combination of rotating frequency and electrical frequency due to the coupling effects of the rotating rotor and the armature reaction in the stator. Moreover, many frequency components appear when the static displacement eccentricity and the static angle eccentricity exist.
(3) When considering the static displacement eccentricity and angle eccentricity together, the dynamic responses will be enlarged and the increase of dynamic displacement response y and dynamic angle response θ_x are irregular due to the

influence of gravity. Many frequency components also can be excited in this case.

Acknowledgement

We would like to express the appreciation to the National Natural Science Foundation of China (Grant No. 51675091), the Major Scientific and Technological Innovation Project of Liaoning Province (Grant No. 201506003), the National Key Foundation for Exploring Scientific Instrument of China (Grant No. 013YQ47076509) to provide financial supports of the research.

References

1. D Dorrell, A Smith, Calculation and measurement of unbalanced magnetic pull in cage induction motors with eccentric rotors, part II: experimental investigation, ***Proceedings of the IEE Electric Power Applications*** 143 (1996) 202–210.
2. TP Holopainen, A Tenhunen, A Arkkio, Electromechanical interaction in rotor vibrations of electric machines, ***Proceedings of the Fifth World Congress on Computational Mechanics*** (2002).
3. L Zhang, Z Ma, B Song, Dynamic characteristics of a rub-impact rotor-bearing system for hydraulic generating set under unbalanced magnetic pull, ***Archive of Applied Mechanics*** 83 (2013) 817–830.
4. T Hattori, K Narita, T Yamada, Influence of harmonic components on electromagnetic vibration for a permanent magnet motor, ***International Conference on Electrical Machines and Systems*****. IEEE**, (2010).
5. ZQ Zhu, ZP Xia, LJ Wu, Analytical modeling and finite-element computation of radial vibration force in fractional-slot permanent-magnet brushless machines, ***Industry Applications IEEE Transactions on*** 46 (2010) 1908-1918.
6. D Torregrossa, et al. Multiphysics finite-element modeling for vibration and acoustic analysis of permanent magnet synchronous machine, ***IEEE Transactions on Energy Conversion*** 26 (2011) 490-500.
7. Lee, Sun Kwon, G. H. Kang, and H. Jin, Finite element computation of magnetic vibration sources in 100 kW two fractional-slot interior permanent magnet machines for ship, ***IEEE Transactions on Magnetics*** 48 (2012) 867-870.
8. B Gaussens, E Hoang, ODL Barriere, Analytical approach for air-gap modeling of field-excited flux-switching machine: no-load operation, ***IEEE Transactions on Magnetics*** 48 (2013) 2505-2517.
9. U Werner, Rotordynamic model for electromagnetic excitation caused by an eccentric and angular rotor core in an induction motor, ***Archive of Applied Mechanics*** 83 (2013) 1215-1238.
10. D Guo, F Chu, D Chen, The unbalanced magnetic pull and its effects on vibration in a three-phase generator with eccentric rotor, ***Journal of Sound and Vibration*** 254 (2002) 297-312.
11. JT Li, ZJ Liu, LHA Nay, Effect of radial magnetic forces in permanent magnet motors with rotor eccentricity, ***IEEE Transactions on Magnetics*** 43 (2007) 2525–2527.

 ISSN 2572-4975 (Print), 2572-4991 (Online)

12. H Im, HH Yoo, J. Chung, Dynamic analysis of a BLDC motor with mechanical and electromagnetic interaction due to air gap variation, ***Journal of Sound and Vibration*** 330 (2011) 1680–1691.
13. M Michon, RC. Holehouse, K Atallah, G Johnstone, Effect of rotor eccentricity in large synchronous machines, ***IEEE Transactions on Magnetics*** 50 (2014) 1-4.
14. DG Dorrell, Sources and characteristics of unbalanced magnetic pull in three-phase cage induction motors with axial-varying rotor eccentricity, ***IEEE Transactions on Industry Applications*** 47 (2011) 12–24.
15. DG Dorrell, JKH Shek, MA Mueller, Damper windings in induction machines for reduction of unbalanced magnetic pull and bearing wear, ***Energy Conversion Congress and Exposition*** 49 (2011) 2206-2216.
16. Y Yu, C Bi, PN Hla, Q Jiang, S Lin, NHA Aung, A Al Mamun, Incline unbalanced magnetic pull induced by misalignment rotor in PMSM, ***IEEE Transactions on Magnetics*** 49 (2013) 2709–2714.
17. C Di, X. Bao, H. Wang，Q Lv, Modeling and analysis of unbalanced magnetic pull in cage induction motors with curved dynamic eccentricity, ***IEEE Transactions on Magnetics*** 51 (2015) 1-7.
18. X Xu, Q Han, F Chu, A four degrees-of-freedom model for a misaligned electrical rotor, ***Journal of Sound and Vibration*** 358 (2015) 356-374.
19. ZQ Zhu, D Howe, Instantaneous magnetic field distribution in brushless permanent magnet DC motors. I. Open-circuit field, ***IEEE Transactions on Magnetics*** 29 (1993) 124-135.
20. ZQ Zhu, D. Howe, Instantaneous magnetic field distribution in brushless permanent magnet DC motors. II. Armature-reaction field, ***IEEE Transactions on Magnetics*** 29 (1993) 136-142.
21. ZQ Zhu, D Howe, Instantaneous magnetic field distribution in brushless permanent magnet DC motors. III. Effect of stator slotting, ***IEEE Transactions on Magnetics*** 29 (1993) 133-151.
22. ZQ Zhu, D Howe, Electromagnetic noise radiated by brushless permanent magnet DC drives, ***Electrical Machines and Drives, 1993. Sixth International Conference on IEEE Xplore*** (1993) 606-611.
23. M Sahraoui, A. Ghoggal, SE Zouzou, ME Benbouzid, Dynamic eccentricity in squirrel cage induction motors – Simulation and analytical study of its spectral signatures on stator currents, ***Simulation Modelling Practice and Theory*** 16 (2008) 1503-1513.